Porosity, Surface Area, Surface Energy, and Hydrogen Adsorption in Nanostructured Carbons

Alejandro Ansón,[†] Jacek Jagiello,[‡] José B. Parra,[§] M. Luisa Sanjuán,[||] Ana M. Benito,[†] Wolfgang K. Maser,[†] and M. Teresa Martínez*,[†]

Instituto de Carboquímica, CSIC, Miguel Luesma Castán 4, 50018 Zaragoza, Spain, Quantachrome Instruments, 1900 Corporate Drive, Boynton Beach, Florida 33426, Instituto Nacional del Carbón, CSIC, Francisco Pintado Fe, 26, 33011 Oviedo, Spain, and Instituto de Ciencia de Materiales de Aragón, CSIC, Universidad de Zaragoza, Facultad de Ciencias, 50009 Zaragoza, Spain

Received: June 24, 2004; In Final Form: August 3, 2004

Hydrogen adsorption isotherms at 77, 87, and 298 K have been measured on three samples of single-wall carbon nanotubes. The highest adsorption capacity (1.58 wt % at 77 K, 1.15 wt % at 87 K, and 0.02 wt % at 298 K) at atmospheric pressure has been observed in a chemically activated sample (activated with KOH), which has hybrid porosity between a carbon nanotube material and a microporous activated carbon. According to CO_2 adsorption at 273 K and density functional theory pore size distributions from N_2 adsorption, it is deduced that pores up to approximately 0.5−0.7 nm can adsorb hydrogen at ambient conditions. Isosteric heat of hydrogen adsorption has been calculated for the three samples, having initial values around 7−7.5 kJ mol^{-1}. It is concluded that the hydrogen adsorption capacity of carbon nanotubes depends both on the extent of their surface area and on the adsorption energy of the surface sites.

I. Introduction

The amount of hydrogen that can be adsorbed by a carbon material depends on its own porosity and the external conditions. The role of the nanostructure in hydrogen adsorption was investigated during the last years and brought out a huge controversy.[1]

Hydrogen adsorption on different high surface activated carbons has been measured at many temperature and pressure conditions.[2−4] Also, nanostructured carbons such as nanofibers (NFs), multiwall nanotubes (MWNTs), and single-wall nanotubes (SWNTs) have been recently probed for hydrogen storage.[5] Many authors have paid special attention to the relation between porosity, surface area, and hydrogen adsorption in these materials. Proportionality between the BET (Brunauer−Emmett−Teller) surface area and hydrogen adsorption in nanostructured carbons has been claimed by some researchers,[6,7] assuming that sorption is surface dependent as in the case of activated carbons. However, in some samples of NFs,[6,8] SWNTs,[9] and open tip MWNTs,[10] the ratio between hydrogen coverage and BET surface was reported to be quite higher than for activated carbons. Structural explanations were proposed for this deviation such as irregularities in NFs detected by H_2 but not by N_2,[8] pressure-induced separation of the SWNTs in the ropes,[9] or the presence of subnanopores.[10]

In effect, the pore shape and width that are preferred for hydrogen storage have been widely discussed. Some discrepancies still exist at this point, perhaps due to the fact that hypothetical storage conditions are not unanimously defined.

In this work, we report hydrogen adsorption data for three samples containing SWNTs. One of them is raw soot produced by the electric arc method, and the others are surface-modified materials obtained from the raw soot. Hydrogen isotherms have been measured at three temperatures up to approximately atmospheric pressure, and the isosteric heat of adsorption has been calculated for the three samples. Nitrogen isotherms at 77 K and CO_2 isotherms at 273 K have been measured, and SWNTs have been characterized by Raman spectroscopy. Based on these data, the influence of surface area and porosity in hydrogen adsorption is discussed.

II. Experimental Methods

The *raw* sample was synthesized in an electric arc reactor with graphite electrodes, using Ni/Y (2/0.5 atomic %) as catalysts.[11] The as-obtained soot, which is collected from the inner walls of the reactor, contains bundles of SWNTs together with some impurities: metallic nanoparticles, amorphous carbon, and graphitic carbon.[12] The raw material was oxidized with air in a furnace at 350 °C for 1 h, under static conditions. This material is here named the *air-treated* sample.

On the other hand, the raw material was also chemically treated with KOH by means of a wet impregnation method in a weight ratio of soot/KOH = 1/4. First of all, KOH was dissolved in 20 mL of water and soot was added to the solution and stirred for 2 h at 60 °C. Subsequently, the material was well dried and heated at 700 °C for 1 h in a N_2 flow of 800 cm^3 min^{-1}. Finally, it was five times washed with 5 M HCl in a stirred vessel and then washed with distilled water in a Soxhlet extractor.

Micro Raman spectra were obtained with a Dilor XY spectrometer using light at 514.5 nm. Raman frequencies were calibrated with the Si line at 520 cm^{-1} and with the peak of highly oriented pyrolytic graphite (HOPG) at 1582 cm^{-1}. The estimated accuracy was 1 cm^{-1}, and the spectral resolution was better than 3 cm^{-1}.

Hydrogen adsorption isotherms for raw, air-treated, and KOH-treated samples were measured using an Autosorb-1 from

* Corresponding author. E-mail: mtmartinez@carbon.icb.csic.es.
[†] Instituto de Carboquímica, CSIC.
[‡] Quantachrome Instruments.
[§] Instituto Nacional del Carbón, CSIC.
[||] Instituto de Ciencia de Materiales de Aragón, CSIC, Universidad de Zaragoza.

10.1021/jp047253p CCC: $27.50
Published on Web 09/08/2004

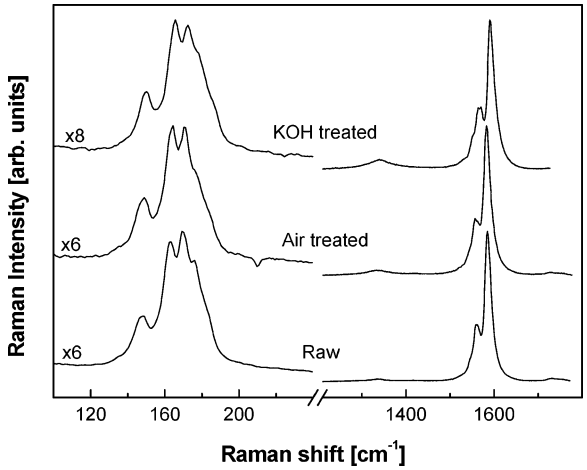

Figure 1. Raman spectra for the raw, air-treated, and KOH-treated samples.

TABLE 1: Main Frequencies that Contribute to the Radial Breathing Mode Signal in the Raman Spectra of the Raw, Air-Treated, and KOH-Treated Samples

raw		air-treated		KOH-treated	
f [cm^{-1}]	d [nm]	f [cm^{-1}]	d [nm]	f [cm^{-1}]	d [nm]
148.0	1.51	148.5	1.51	149.5	1.50
163.0	1.37	163.9	1.36	165.0	1.36
169.8	1.32	170.8	1.31	172.6	1.30
176.0	1.27	175.8	1.27	178.8	1.25

Quantachrome Instruments. CO_2 isotherms and N_2 isotherms were measured in Autosorb-1 and ASAP 2010 from Micromeritics. The samples, of about 110 mg, were degassed at 250 °C under a vacuum.

III. Raman Characterization

Raman spectroscopy is a powerful tool for the characterization of the SWNTs. One of the interesting features in the Raman spectrum of the SWNTs is the appearance of the *radial breathing modes* (RBMs), whose frequencies depend on the diameter of the SWNTs. This dependence has been expressed as $f_b = 223.75/d$, where f_b is the frequency in cm^{-1} and d is the diameter of the SWNT in nm.[13] According to this expression, the diameter of the nanotubes in the raw, air-treated, and KOH-treated samples has been calculated. Figure 1 shows the Raman spectra for the three samples. In this plot, Raman intensity is normalized to show clearly the shape of the spectra. As indicated in Figure 1, the intensities in the RBM zone (120−220 cm^{-1}) are multiplied by a factor of 6−8 related to the intensities in the tangential mode zone (1200−1800 cm^{-1}). The RBM signal was separated into the main contributive frequencies, which correspond to SWNT diameters ranging from 1.2 to 1.5 nm (Table 1). The frequencies of the RBMs for the three samples are almost the same, and only a decrease in the intensity is observed for the treated samples (not shown in Figure 1 due to the normalized intensities). This means that some SWNTs are modified or destroyed during the treatments but there is not a diameter selective destruction. In conclusion, the three samples have SWNTs, whose inner cavities are cylindrical pores with diameter about 1.2−1.5 nm, where gases could be adsorbed.

IV. N_2 and CO_2 Adsorption

Figure 2a shows the nitrogen adsorption isotherms at 77 K for the three samples. The raw sample exhibits a type II isotherm, according to the IUPAC classification. The isotherm

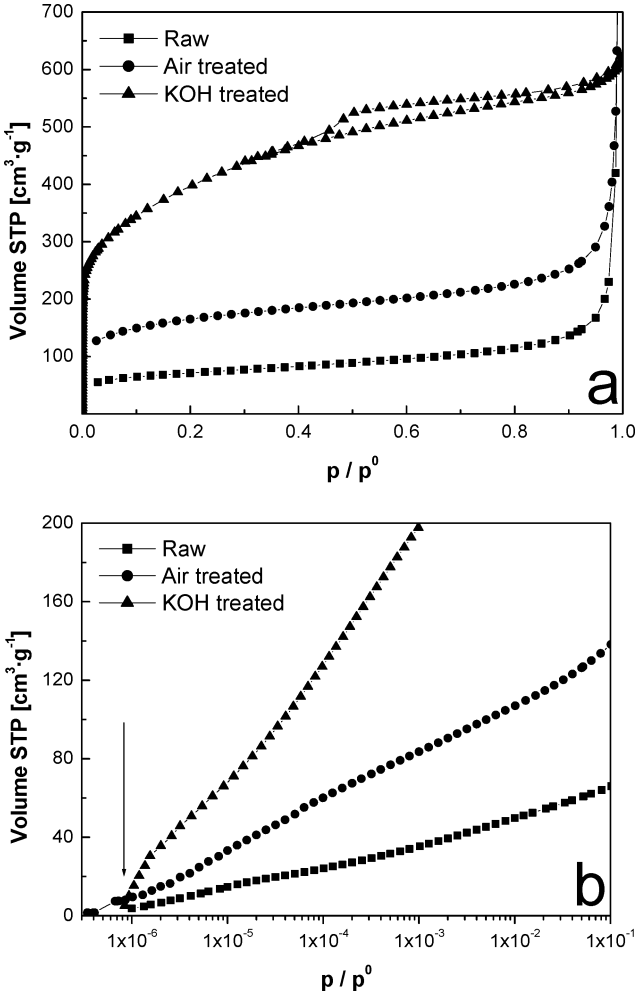

Figure 2. Nitrogen isotherms at 77 K for raw, air-treated, and KOH-treated samples: (a) linear scale; (b) semilogarithmic scale showing the zone of very low relative pressures, where the isotherms cross (marked with an arrow).

presents an initial steep increase in adsorption because there are micropores in the raw sample. This fact has been previously reported for the same material.[14] A narrow hysteresis loop (not shown in Figure 2) appears at very high relative pressures, around 0.9, together with the high increase in the adsorption. The air-treated sample also presents a type II isotherm with similar features to the isotherm of the raw sample, although it has a higher increase in adsorption at the initial step, due to the developed microporosity. The isotherm for the KOH-treated sample is type IV with a hysteresis loop at relative pressures higher than 0.4. However, the more characteristic feature of the curve is the steep increase at low relative pressures that is indicative of a microporous material.

Figure 2b is a semilogarithmic plot of the nitrogen isotherms that allows us to appreciate differences between the three samples at very low relative pressures. The KOH-treated sample adsorbs more nitrogen at almost any pressure, but around 10^{-6} the isotherm crosses the isotherm of the air-treated sample. Although in the limiting zone of the very low relative pressures the precision of the measurement devices becomes worse, the crossing of the isotherms is noticeable. More data about this feature will be shown below.

More information about the low relative pressure region can be derived from the CO_2 isotherms at 273 K, which are plotted for the three samples in Figure 3. In this plot, it is seen that the air-treated sample adsorbs more CO_2 than the KOH-treated

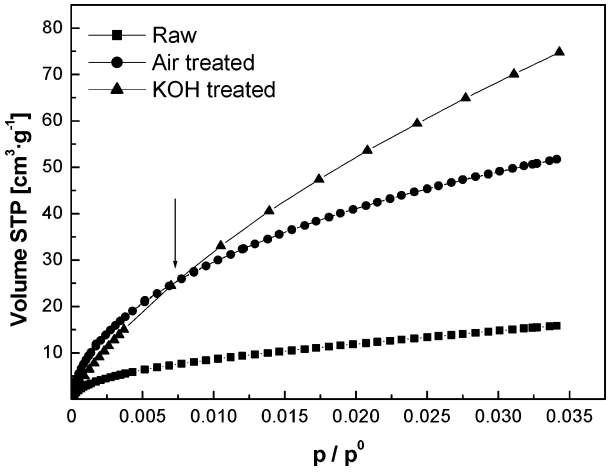

Figure 3. Carbon dioxide isotherms at 273 K for raw, air-treated, and KOH-treated samples.

TABLE 2: Some Parameters of Porosity for the Three Samples: S BET, Specific Surface Area; V_{Mi}, Micropore Volume; E_0, Characteristic Energy; L, Average Micropore Size; q, Exponent of the DA Equation

sample	raw	air-treated	KOH-treated
S BET [m^2 g^{-1}]	262	552	1433
V_{Mi} (DR, N_2) [cm^3 g^{-1}]	0.0830	0.1995	0.5366
V_{Mi} (DR, CO_2) [cm^3 g^{-1}]	0.0448	0.1592	0.2321
V_{Mi}(DR, N_2) − V_{Mi}(DR, CO_2)	0.0382	0.0403	0.3045
E_0 (DR, CO_2) [kJ mol^{-1}]	22.52	21.76	18.92
L (DR, CO_2) [nm]	0.97	1.04	1.43
V_{Mi} (DA, CO_2) [cm^3 g^{-1}]	0.0794	0.2699	0.8307
q (DA exponent, CO_2)	1.40	1.46	1.29
E_0 (DA, CO_2) [kJ mol^{-1}]	15.96	16.03	10.33

sample at relative pressures below 0.008 and the KOH-treated sample adsorbs more CO_2 at higher relative pressure. The crossing point between the isotherms for the air-treated and KOH-treated samples, which is marked with an arrow in Figure 3, occurs at a relative pressure higher than in the case of N_2 isotherms at 77 K (Figure 2b). This fact is usually explained as a kinetically favored adsorption of CO_2 at 273 K compared to N_2 adsorption at 77 K, which is rather slower due to the low temperature.[15]

Several parameters regarding microporosity have been calculated from data of N_2 adsorption at 77 K and CO_2 adsorption at 273 K (Table 2). The BET surface area[16] (S BET) has been calculated from N_2 adsorption data at relative pressures between 0.01 and 0.1 approximately, where the BET isotherm[16] is linear. This relative pressure zone corresponds to the initial steep increase in isotherms in Figure 2a. In fact, the BET surface area increases by a factor of 2 in the air-treated sample compared to the raw and by a factor of 5.5 in the case of the KOH-treated sample. This is similar to the variation observed in isotherms in Figure 2a.

The change with activation in the Dubinin−Radushkevich (DR) micropore volume (V_{Mi}) from N_2 adsorption data behaves as expected, in the same manner as the BET surface area because micropores are mainly responsible for the total surface area. The DR equation[17] has been used in the usual form:

$$W = W_0 \exp\left[-\left(\frac{RT}{\beta E_0}\ln\left(\frac{p^0}{p}\right)\right)^q\right] \qquad q = 2$$

where W is the amount of adsorbate at temperature T and relative pressure p/p^0, W_0 is the amount of adsorbate in micropores, β is the affinity coefficient (0.48 for CO_2 and 0.34 for N_2), and

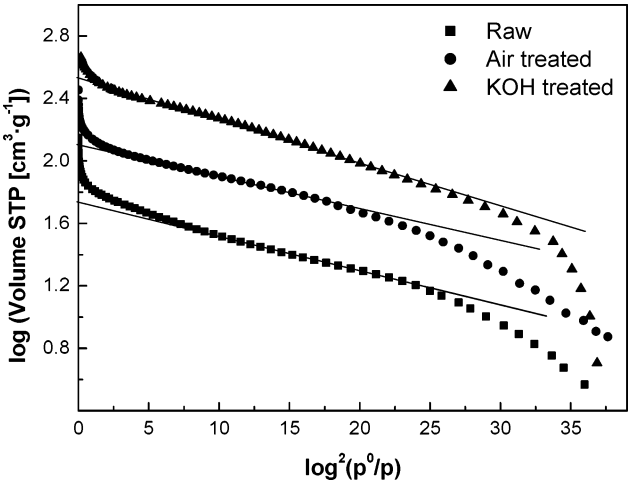

Figure 4. Dubinin−Radushkevich plot from the N_2 adsorption data at 77 K.

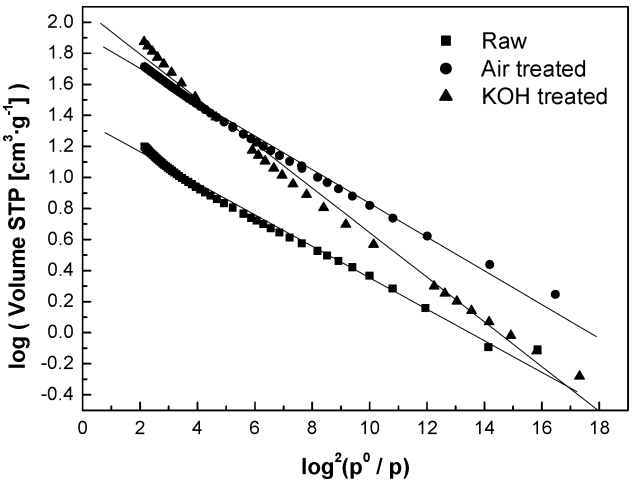

Figure 5. Dubinin−Radushkevich plot from the CO_2 isotherm data at 273 K.

E_0 is the characteristic energy. Figure 4 shows the DR plots from the N_2 adsorption data for the three samples. In this case, no crossing is observed between the plots in the linear regions.

The DR micropore volume from the CO_2 adsorption data at 273 K is useful for the assessment of narrow microporosity (width below 0.7 nm).[18] Figure 5 is the CO_2 DR plot for the three samples, which have nearly linear tendencies. The plot also shows clearly how the isotherm for the KOH-treated sample passes across those for the air-treated and raw samples. The difference between the N_2 DR micropore volume and the CO_2 DR micropore volume increases noticeably for the KOH-treated sample, indicating that the peak of the micropore size distribution has moved to wider diameters. An estimate of the average micropore size can be obtained according to the expression L (nm) = $10.8/(E_0 - 11.4)$.[19] The average micropore size for the KOH-treated sample appears at 1.43 nm, that is, 0.4 nm larger diameter than for the other samples.

The Dubinin−Astakhov (DA) equation[17] can be used to improve the DR linear fitting for the isotherm data, as can be observed in Figure 6. The DA equation is the same as the DR expression, but allowing the exponent q to be different from 2. The found exponents for the raw, air-treated, and KOH-treated samples are included in Table 2, together with the values for E_0 and the DA micropore volume. The KOH-treated sample needs the lowest exponent q and is the most different from the DR $q = 2$.

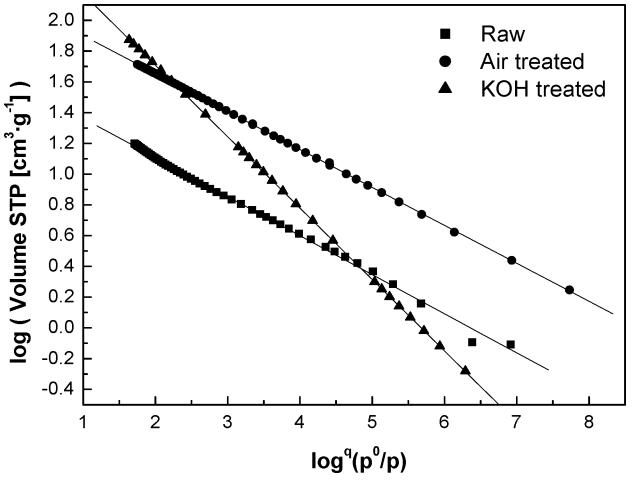

Figure 6. Dubinin−Astakhov plot from the CO_2 isotherm data at 273 K.

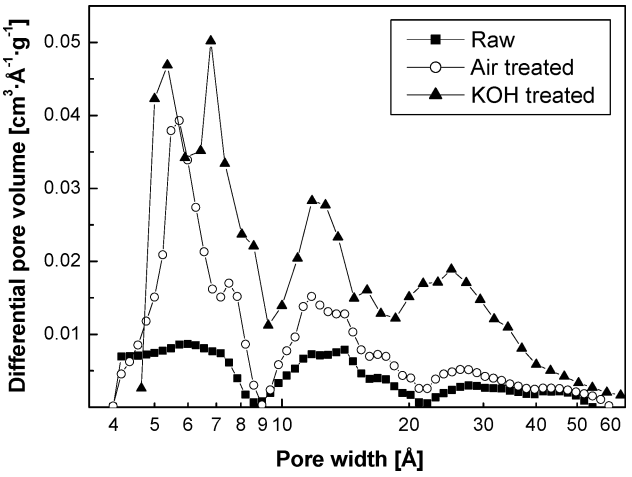

Figure 7. DFT pore size distributions from the N_2 isotherms at 77 K.

V. Density Functional Theory Interpretation

Detailed pore size distributions shown in Figure 7 were calculated for the three samples from their N_2 adsorption isotherms using the density functional theory (DFT) method. General information about the method can be found elsewhere.[20,21] The implementation of the method used in this work was developed by Neimark and co-workers.[22] It is available in the Autosorb-1 software [Quantachrome Instruments]. The calculated pore size distributions (Figure 7) allow explanation of adsorption isotherms in relation to pore sizes taking into account that narrow pores represent the high energy adsorption sites that can adsorb gas molecules at very low equilibrium pressures. The distribution for the KOH-treated sample crosses that for the air-treated sample at about 0.5 nm. According to this calculation, the air-treated sample has more pores smaller than 0.5 nm width than the KOH-treated sample, although this sample has much higher total micropore volume. The raw sample has also more small micropores (less than 0.5 nm) than the KOH-treated sample and possibly more small micropores (less than 0.45 nm) than the air-treated sample. The DFT shows a shift of the average micropore diameter toward larger values with the KOH activation, which is in agreement with the results obtained from the CO_2 isotherms (Table 2). In fact, maxima around 0.6 nm appear for the raw and the air-treated samples and a peak at around 0.7 nm (absolute maximum) is observed in the distribution for the KOH-treated sample.

Most of the SWNTs in the raw sample are closed at their ends so the inner cavities do not have an important contribution to gas adsorption. In fact, for the raw sample, the pore size distribution shows a homogeneous dispersion of widths (the minima at around 1 and 2 nm are not real but are a consequence of the mathematical limitations of the DFT method). The interstitial cavities in the bundles of SWNTs, with pore widths of 0.2−0.3 nm, are not seen by N_2 at 77 K. When SWNTs are oxidized with air, the nanotube tips are broken and the inner cavities become accessible to gases.[14] In the DFT pore size distribution, this would correspond to an increase in the number of pores of widths between approximately 1.2 and 1.5 nm. In fact, an increase in the number of pores of such width is observed for the air-treated sample. However, an appreciable amount of pores of about 0.6 nm appear in the distribution. These sites could be assigned to inner cavities of SWNTs with smaller effective diameter. For example, some SWNTs may have their open tips partially blocked by oxygenated groups that are introduced with the oxidation process. This possibility has been studied for Xe adsorption in SWNTs.[23] An activation of other sites in the sample impurities, such as the amorphous and graphitic carbon, must be also taken into account.

In the KOH-activated sample, the SWNTs are probably broken and the gas can access the inner cavities, which can be partially blocked by oxygenated groups. In the KOH-activated sample, a noticeable increase is observed in the amount of mesopores which could be due to the activation of amorphous and graphitic carbon. The KOH-treated sample has hybrid porosity between a nanotube material and an activated carbon. It has wider pores and higher surface area than the raw and the air-treated samples.

VI. H_2 Adsorption

Hydrogen adsorption isotherms were measured for the raw, air-treated, and KOH-treated samples at 77, 87, and 298 K and up to nearly atmospheric pressure. The highest hydrogen capacity at atmospheric pressure was found for the KOH-treated sample at the three temperatures (1.58 wt % at 77 K, 1.15 wt % at 87 K, and 0.02 wt % at 298 K). On the other hand, the adsorption is higher at the lowest temperature, as is expected in a physisorption mechanism. In passing from 77 to 87 K, the adsorption decreases noticeably. At 298 K, the adsorption is very low.

Figure 8 is a comparison of the hydrogen isotherms obtained for the three samples at the same temperatures. At 77 K, when the isotherms are plotted in the usual linear way, the situation looks quite similar to N_2 isotherms in Figure 2a. The KOH-treated sample adsorbs more H_2 than the air-treated sample, and this one adsorbs more than the raw sample. However, when the isotherms are plotted in a double-logarithmic scale, the low-pressure region is magnified and the relative positions of the isotherms vary. At about 2−3 Torr, the isotherm for the KOH-treated sample crosses that for the air-treated sample. This sample adsorbs more H_2 than the others at pressures less than 2−3 Torr. The crossing of the isotherms is similar to the crossing observed for N_2 in Figure 2b and for CO_2 in Figure 3. For N_2 adsorption at 77 K, the crossing occurs at absolute pressures much lower than in the case of H_2 at 77 K. The crossing between the isotherms for the KOH-treated sample and the air-treated sample can be interpreted as pressure points in which the adsorption potential is equal for both samples. This has also an interpretation according to the pore size distributions shown in Figure 7, where the KOH-treated line crosses the air-treated line at about 0.5 nm: pores of about 0.5 nm width start

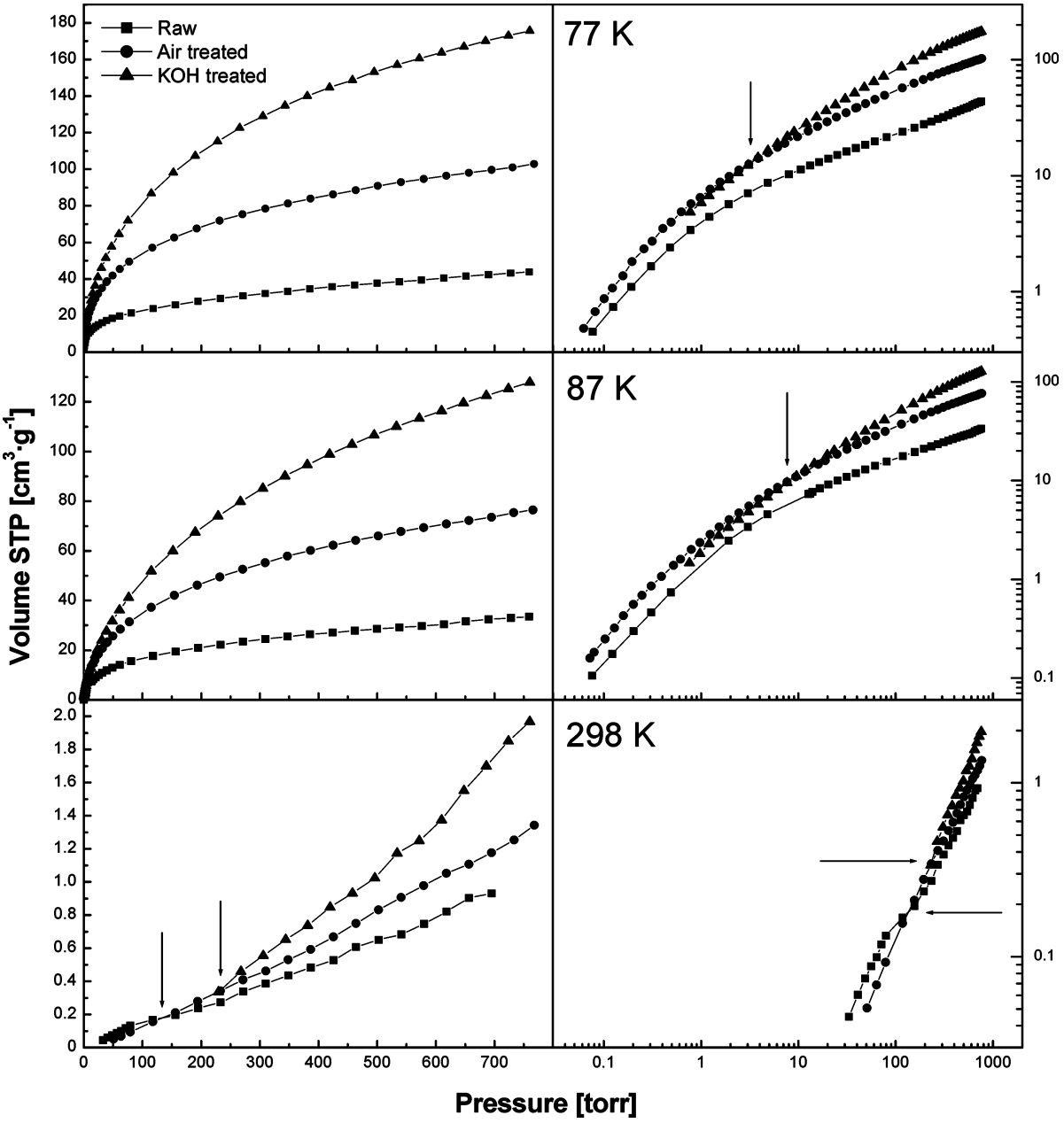

Figure 8. Experimental adsorption isotherms of hydrogen on raw, air-treated, and KOH-treated samples at 77, 87, and 298 K. Isotherms are plotted in linear scale (left) and double-logarithmic scale (right) in order to show clearly the whole range of the measurements. Lines between experimental points are drawn to guide the eye. Arrows point to sites where the isotherms cross.

adsorbing hydrogen at 77 K at a minimum pressure of approximately 2−3 Torr.

A very similar situation is observed for H_2 isotherms at 87 K. In the double-logarithmic plot, the KOH-treated isotherm also crosses the air-treated isotherm. The difference is only a scaling factor due to the temperature change. The isotherm crossing is observed at about 10 Torr, so pores of 0.5 nm start adsorbing H_2 at a minimum pressure of 10 Torr.

At 298 K, the change in the H_2 isotherm plot is more noticeable. The crossing of the isotherms is easily appreciable directly in the normal linear plot. The KOH-treated isotherm crosses the air-treated isotherm at about 250 Torr, so pores of 0.5 nm can adsorb H_2 at a minimum pressure of 250 Torr at 298 K. The air-treated isotherm also crosses the raw isotherm, so pores of about 0.45 nm adsorb H_2 at a minimum pressure of about 125 Torr at 298 K.

The large temperature difference between cryogenic and ambient conditions implies important changes in the chemical potential of the gas that must be compensated with a pressure increment. Since the chemical potential is proportional to the natural logarithm of pressure, the variation can be directly evaluated from the logarithmic isotherm plots.

In viewing all these isotherms at different temperatures and with different adsorbates, it becomes clear that the same physisorption phenomenon is present at this range of conditions. Variations of pressure and temperature are only changes in the scale, as already suggested by Polanyi with his idea of a characteristic curve.[24] The zone of the characteristic curve and the magnification can be changed with the conditions or the adsorbate. N_2 at 77 K gives the complete characteristic isotherm although for a detailed study of the low relative pressure region other adsorbates such as CO_2 at 273 K[15] are necessary. Hydrogen isotherms at ambient temperature have been also claimed as a method for the magnification of the low relative pressure region in the N_2 isotherm at 77 K.[25] Here we have seen an example.

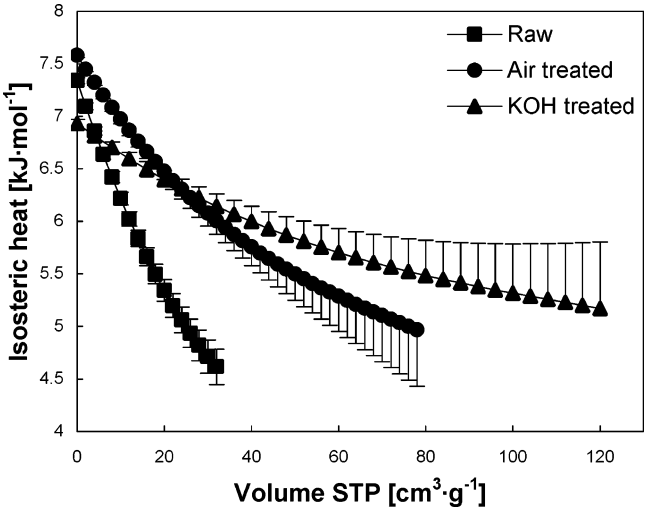

Figure 9. Variation of the hydrogen isosteric heat of adsorption with the coverage for the raw, air-treated, and KOH-treated samples.

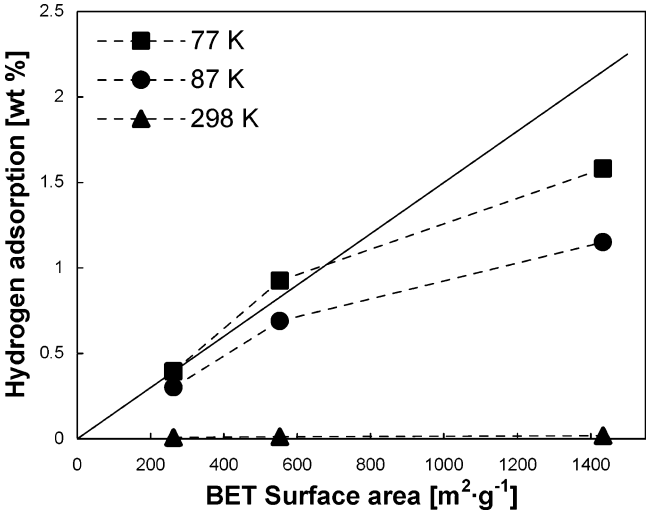

Figure 10. Comparison between the BET surface area and the hydrogen adsorption at 77, 87, and 298 K and nearly atmospheric pressure for the raw (262 m^2 g^{-1}), air-treated (552 m^2 g^{-1}), and KOH-treated (1433 m^2 g^{-1}) samples. The solid line represents an empirical relation obtained from electrochemical adsorption of hydrogen on many carbon samples (ref 7).

The experimental hydrogen isotherms were described and analyzed using the following form of the virial equation:

$$\ln p = \ln v + \frac{1}{T}\sum_{i=0}^{m} a_i v^i + \sum_{i=0}^{n} b_i v^i \qquad (1)$$

where v, p, and T are the amount adsorbed, pressure, and temperature, respectively, and a_i and b_i are empirical parameters. Properties of this equation were discussed elsewhere.[26,27] Here it is used to calculate the isosteric heats of hydrogen adsorption on raw, air-treated, and KOH-treated samples. The isosteric heat of adsorption, Q_{st}, is obtained from adsorption isotherms measured at different temperatures by applying the following expression:

$$Q_{st} = -R\sum_{i=0}^{m} a_i v^i \qquad (2)$$

where R is the universal gas constant. The isosteric heats of adsorption calculated using eq 2 and the fitted parameters are shown for the three samples in Figure 9. Error bars in the plots represent standard deviations of the Q_{st} values estimated from variances of parameters calculated from the data fitting procedure. For clarity in Figure 9, only (+) error bars and (−) error bars are plotted for the KOH-treated and the air-treated samples, respectively.

Isosteric heat of adsorption decreases with the coverage in agreement with previously reported results for methane adsorption on SWNTs.[28] Results in this previous report showed a bit higher values for the zero coverage isosteric heat, around 13.8 kJ mol^{-1}. The air-treated sample has the highest initial isosteric heat of hydrogen adsorption (7.58 kJ mol^{-1}), while the KOH-treated sample has the lowest (6.93 kJ mol^{-1}). The raw sample has an intermediate value (7.34 kJ mol^{-1}). Nevertheless, at higher coverages the KOH-treated sample has the highest values of heat of adsorption. The crossing tendencies in the heat of adsorption for the samples are related to a change in the energy site distribution, that is, a change in the pore size distribution, as discussed above.

VII. Discussion

The KOH-treated sample has less high energy sites than the other two samples. In consequence, the KOH-treated sample adsorbs less hydrogen at ambient temperature when pressure is lower than 125 Torr. Nevertheless, it adsorbs more hydrogen at atmospheric pressure because other less energetic sites can adsorb at this pressure and the KOH-treated sample has a larger amount of these sites and thus higher BET surface area (N_2, 77 K). According to the data in Figures 7 and 8, the best material to adsorb hydrogen at 298 K and atmospheric pressure would have micropores that should be a bit larger than 0.5 nm of maximum width and as dense as possible. Obviously, the pores do not have to be necessarily of 0.2−0.3 nm, as sometimes is proposed. And this is important because it is normally difficult to increase the surface area of a given carbon material without increasing the average micropore width.

A more developed surface area can compensate the lack of high energy sites at the appropriate conditions. Moreover, the presence of wide micropores can compensate the lack of more energetic sites if the conditions are adequate for the filling mechanism: after covering the surface of the pore, the adsorbate can occupy the interior space. This is the case of super high surface area carbons, which have BET surface areas (N_2, 77 K) of more than 2000 m^2 g^{-1}.

Figure 10 is a comparison between the BET surface area and the hydrogen adsorption at 77, 87, and 298 K and nearly atmospheric pressure for the raw, air-treated, and KOH-treated samples. The solid line represents an empirical relation obtained from electrochemical adsorption of hydrogen on many carbon samples.[7] In the electrochemical adsorption, an external energy is supplied to get the adsorption of hydrogen from an aqueous solution over the carbonaceous electrode at room conditions. This mechanism is surface area dependent, and the surface can be saturated with hydrogen by supplying enough current at the adequate voltage. In Figure 10, at 77 K the points for the raw and the air-treated samples fall approximately over the solid line, so a monolayer of hydrogen is probably near completion at atmospheric pressure. The point for the KOH-treated sample falls below the solid line due to the widening of the micropore size distribution. Larger pores need higher pressure or lower temperature for H_2 than for N_2 to adsorb, and the filling mechanism is more active in the case of N_2 at 77 K. At 87 K, the monolayer is farther from completion and the points in Figure 10 for the three samples are separated from the solid

electrochemical line. At 298 K, the three points are far from the solid line. At the three temperatures, the physisorption of hydrogen at atmospheric pressure seems proportional to the BET surface but the proportionality changes with temperature. And if the conditions are allowed to vary in a wide range (lower pressure and/or higher temperature), the hydrogen adsorption may be not proportional to the BET surface area.

Now the above discussion can be extended to the conditions of the hydrogen storage, for example, ambient temperature and pressures between 50 and 100 bar. Clearly, micropores wider than those that can adsorb at atmospheric pressure can adsorb at 50 bar. In other words, less energetic sites can adsorb at such pressures, and they will adsorb more hydrogen than high energy sites if they can accommodate a larger number of hydrogen molecules. For example, a nanotube is probably a deeper potential well than a slit-shaped pore but molecular simulation of hydrogen adsorption predicts more hydrogen adsorption in the slits at high pressures.[29] In fact, recent experiments of H_2 adsorption on carbon nanotubes at high pressure[30,31] only found moderate gas uptakes.

Finally, for storage purposes, not only adsorption but also desorption must be taken into account. From DFT data, it is known that pores of 0.5−0.7 nm retain hydrogen at ambient temperature and pressure. So if hydrogen adsorbed in pores of less than 0.5 nm diameter needs to be released at external atmospheric pressure, heating the sample will probably be necessary.

VIII. Conclusions

Similarities between the adsorption isotherms for N_2, CO_2, and H_2 are in accordance with physisorption of gases over the surface of the SWNT samples. Since physisorption is a two-dimensional process, it is surface dependent and the adsorption depends on both the adsorption potential and the extent of the surface area.

If several surfaces that are close to being saturated with adsorbate are compared, the highest adsorption normally corresponds to the largest surface material. Nearly saturated surfaces can be reached, for example, by means of electrochemical adsorption of hydrogen or gas adsorption at cryogenic temperatures. In fact, the KOH-treated sample has the highest surface area (S BET = 1433 $m^2\ g^{-1}$) and adsorbs 1.58 wt % H_2 at 77 K and 760 Torr. This is much more than the amount adsorbed by the raw sample at the same conditions.

If the monolayer is not completed and, moreover, it is in the initial stage of coverage, the amount of adsorbate depends on the strength of the adsorption sites (the micropore width). The raw and air-treated samples have more very small micropores and can keep more gas than the KOH-treated sample at low pressure and high temperature. Good information about the initial step of the adsorption is provided by the low coverage isosteric heat of adsorption. This magnitude is usually similar to that of the adsorption energy at ambient temperature. For the arc-produced SWNTs, the low coverage isosteric heat of H_2 adsorption has values around 7−7.5 kJ mol^{-1}.

Based on DFT pore size distributions from N_2 adsorption data at 77 K, it is deduced that hydrogen can be adsorbed in pores with a maximum width of 0.5−0.7 nm at room temperature.

Acknowledgment. This work was supported by the CSIC Fuel Cell Network and the Spanish MCYT Project NANOENER MCYT; MAT2002-04630-C02-01.

References and Notes

(1) Dagani, R. *Chem. Eng. News* **2002**, *80* (2), 25−28.
(2) Amankwah, K. A. G.; Noh, J. S.; Schwarz, J. A. *Int. J. Hydrogen Energy* **1989**, *14* (7), 437−447.
(3) Chahine R.; Bose, T. K. *Int. J. Hydrogen Energy* **1994**, *19* (2), 161−164.
(4) Zhou, L.; Zhou, Y. *Sci. China* (*Ser. B*) **1996**, *39* (4), 598−607.
(5) Hirscher, M.; Becher, M. *J. Nanosci. Nanotechnol.* **2003**, *3*, 3−17.
(6) Ströbel, R.; Jörissen, L.; Schliermann, T.; Trapp, V.; Schütz, W.; Bohmhammel, K.; Wolf, G.; Garche, J. *J. Power Sources* **1999**, *84*, 221−224.
(7) Züttel, A.; Sudan, P.; Mauron, P.; Wenger, P. *Appl. Phys. A* **2004**, *78*, 941−946.
(8) Ahn, C. C.; Ye, Y.; Ratnakumar, B. V.; Witham, C.; Bowman, R. C., Jr.; Fultz, B. *Appl. Phys. Lett.* **1998**, *73* (23), 3378−3390.
(9) Ye, Y.; Ahn, C. C.; Witham, C.; Fultz, B.; Liu, J.; Rinzler, G.; Colbert, D.; Smith, K. A.; Smalley, R. E. *Appl. Phys. Lett.* **1999**, *74* (16), 2307−2309.
(10) Gao, H.; Gu, X. B.; Li, J. T.; Wu, G. T.; Yin, J. L.; Wu, K.; Xu, D. S. *Appl. Phys. Lett.* **2003**, *83* (16), 3389−2391.
(11) Journet, C.; Maser, W. K.; Bernier, P.; Loiseau, A.; Lamy de la Chapelle, M.; Lefrant, S.; Deniard, P.; Lee, R.; Fischer, J. E. *Nature* **1997**, *388*, 756−758.
(12) Martínez, M. T.; Callejas, M. A.; Benito, A. M.; Cochet, M.; Seeger, T.; Ansón, A.; Schreiber, J.; Gordon, C.; Marhic, C.; Chauvet, O.; Maser, W. K. *Nanotechnology* **2003**, *14*, 691−695.
(13) Bandow, S.; Asaka, S.; Saito, Y.; Rao, A. M.; Grigorian, L.; Richter, E.; Eklund, P. C. *Phys. Rev. Lett.* **1998**, *80* (17), 3779−3782.
(14) Fujiwara, A.; Ishii, K.; Suematsu, H.; Kataura, H.; Maniwa, Y.; Suzuki, S.; Achiba, Y. *Chem. Phys. Lett.* **2001**, *336*, 205−211.
(15) Garrido, J.; Liares-Solano, A.; Martín-Martínez, J. M.; Molina-Sabio, M.; Rodríguez-Reinoso, F.; Torregrosa, R. *Langmuir* **1987**, *3*, 76−81.
(16) Rouquerol, F.; Rouquerol, J.; Sing, K. *Adsorption by Powders and Porous Solids*; Academic Press: London, 1999; pp 166−174.
(17) Rouquerol, F.; Rouquerol, J.; Sing, K. *Adsorption by Powders and Porous Solids*; Academic Press: London, 1999; pp 110−112.
(18) Lozano-Castelló, D.; Cazorla-Amorós, D.; Linares-Solano, A. *Carbon* **2004**, *42*, 1233−1242.
(19) Stoeckli, F.; Ballerini, L. *Fuel* **1991**, *70*, 557−559.
(20) Tarazona P.; Marini Bettolo Marconi, U.; Evans, R. *Mol. Phys.* **1987**, *60*, 573−595.
(21) Lastoskie, C.; Gubbins, K. E.; Quirke, N. *J. Phys. Chem.* **1993**, *97*, 4786−4796.
(22) Ravikovitch, P. I.; Vishnyakov, A.; Russo, R.; Neimark, A. V. *Langmuir* **2000**, *16*, 2311−2320.
(23) Kuznetsova, A.; Yates, J. T.; Simonyan, V. V.; Johnson, J. K.; Huffman, C. B.; Smalley, R. E. *J. Chem. Phys.* **2001**, *115* (14), 6691−6698.
(24) Young, D. M.; Crowell, A. D. *Physical Adsorption of Gases*; Butterworth: London, 1962; pp 137−140.
(25) Koresh, J. E. *J. Chem. Soc., Faraday Trans.* **1993**, *89* (12), 2059−2062.
(26) Jagiello, J.; Bandosz, T. J.; Putyera, K.; Schwarz, J. A. *J. Chem. Eng. Data* **1995**, *40*, 1288−1292.
(27) Jagiello, J.; Bandosz, T. J.; Schwarz, J. A. *Langmuir* **1996**, *12*, 2837−2842.
(28) Talapatra, S.; Migone, A. D. *Phys. Rev. B* **2002**, *65*, 045416.
(29) Wang, Q.; Johnson, J. K. *J. Chem. Phys.* **1999**, *110* (4), 577−586.
(30) Gundiah, G.; Govindaraj, A.; Rajalakshmi, N.; Dhathathreyan, K. S.; Rao, C. N. R. *J. Mater. Chem.* **2003**, *13*, 209−213.
(31) Smith, M. R.; Bittner, E. W.; Shi, W.; Johnson, J. K.; Bockrath, B. C. *J. Phys. Chem. B* **2003**, *107*, 3752−3760.